

基于涂覆石墨烯量子点-聚乙烯醇的拉锥细芯光纤的温湿度传感器

鲁志琪, 董锐敏, 刘昌宁*

湖北师范大学物理与电子科学学院, 湖北 黄石 435002

摘要 提出了一种基于拉锥细芯光纤的温湿度传感器。先将细芯光纤熔接在两段多模光纤的中间,并在多模光纤两端熔接单模光纤,利用拉锥机对细芯光纤进行分步拉锥。实验测得细芯光纤拉锥前后的传感器的温度灵敏度分别为 $31 \text{ pm}/^\circ\text{C}$ 和 $72.7 \text{ pm}/^\circ\text{C}$ 。将少量石墨烯量子点-聚乙烯醇涂覆在传感器锥部得到温湿度传感器,实验测得其温度灵敏度最大为 $288.3 \text{ pm}/^\circ\text{C}$,湿度灵敏度可达到 $131.7 \text{ pm}/\%$ 。该传感器具有性能稳定、灵敏度高、制备简单、成本低的特点,在温度和湿度传感领域具有广阔的应用前景。

关键词 传感器; 细芯光纤; 石墨烯量子点; 聚乙烯醇; 温度; 相对湿度

中图分类号 TN253 **文献标志码** A

DOI: 10.3788/CJL220717

1 引言

温度与相对湿度作为传感研究中的重要参数,已被广泛应用于环境监测与生物化学研究领域。各种温湿度传感器相继问世,例如传统温湿度计、全碳基传感器^[1]以及光纤传感器。其中的光纤传感器凭借其耐高温、耐腐蚀、灵敏度高等优点在各领域获得了广泛研究与应用,并在航天、医疗、环境等领域实现了温度和湿度的实时监测^[2-8]。

光纤传感器可以分为功能性传感器^[9]和非功能性传感器^[10]。功能性传感器中的光纤不仅可以使整个传感结构更加紧凑,而且不需要另外增设其他光敏元件;同时,在光纤的传感部分涂覆温敏、湿敏材料可以进一步提高传感器的灵敏度。因此,功能性传感器成为光纤传感研究的重点。光纤温湿度传感器主要以光栅型传感器^[11-14]和干涉型传感器^[15-17]为主。相较于灵敏度普遍较低的光栅型传感器,干涉型传感器具有制备简单、灵敏度高优点,在温度传感^[18-21]、湿度传感^[22-25]、折射率传感^[26-28]、应力传感^[29-30]等领域被广泛应用与研究。

2009年时,Lu等^[31]先将一段光子晶体光纤拉锥,然后将其与长周期光栅级联,构成马赫-曾德尔干涉仪(MZI),该传感器的温度灵敏度为 $69.3 \text{ pm}/^\circ\text{C}$ 。为了提高温度传感器的灵敏度,2019年时,Gong等^[32]将

聚二甲基硅氧烷(PDMS)薄膜涂覆在互相错位熔接的三段单模光纤上,将传感器的温度灵敏度提高到了 $101 \text{ pm}/^\circ\text{C}$ 。2019年,Vaz等^[33]通过在单模光纤中拼接一个短的空心硅管形成法布里-珀罗(FP)腔结构,然后将聚乙烯醇(PVA)涂覆到传感部分,得到了相对湿度灵敏度为 $32.54 \text{ pm}/\%$ 。2021年,徐妍妍等^[34]将七芯光纤熔接至两段单模光纤之间(单模-七芯-单模),并将亲水材料氧化石墨烯涂覆在熔融拉锥过后的七芯光纤锥部,使传感器的相对湿度灵敏度达到 $53.5 \text{ pm}/\%$ 。

近年来,石墨烯量子点(GQDs)^[35-36]这种新型的纳米材料以其优异的光学性质与生物化学性能引起了各领域研究人员的极大关注。聚乙烯醇^[37-38]是一种根据周围环境湿度不同而改变自身折射率的溶液。将石墨烯量子点与聚乙烯醇混合后涂覆至传感部分可以同时提高传感器对温湿度的灵敏度。

本团队设计并制备了一种基于石墨烯量子点-聚乙烯醇涂覆的锥形细芯光纤的温湿度传感器。首先将两段多模光纤(MMF)与细芯光纤(TCF)进行级联,然后采用熔接机对细芯光纤进行分步拉锥(由于包层模式之间发生干涉形成了马赫-曾德尔干涉仪,因此该结构对外部环境参数的改变较未拉锥时更为敏感),最后将石墨烯量子点-聚乙烯醇溶液涂覆在细芯光纤锥部并进行加热处理。加热处理结束后,石墨烯量子点-聚乙烯醇以薄膜状

收稿日期: 2022-03-30; 修回日期: 2022-04-14; 录用日期: 2022-04-19; 网络首发日期: 2022-04-29

基金项目: 湖北省高等学校优秀中青年科技创新团队计划项目(T2020014, T2021010)、湖北师范大学省级大学生创新创业训练计划项目(S202210513051)

通信作者: *liusir1001@163.com

贴附于传感部分的表面。测试该传感器的温度灵敏度、相对湿度灵敏度以及稳定性,结果表明,该传感器具有优异的温湿度灵敏度,且该传感器具有制备方法简单、成本低、灵敏度高、线性度好、稳定性强等优点,在温度与湿度传感领域具有很大的发展潜力。

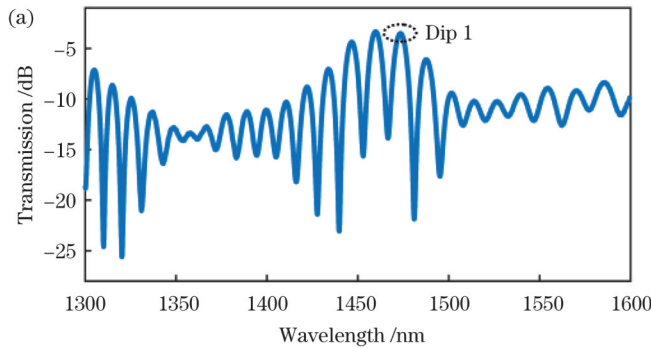
2 传感器制备与理论分析

2.1 传感器的结构设计与制备

实验中使用的是日本藤仓公司生产的光纤熔接机。所使用的各种光纤均由长飞光纤光缆股份有限公司生产,其中单模光纤(SMF)的芯径为 $9\ \mu\text{m}/125\ \mu\text{m}$,多模光纤的芯径为 $62.5\ \mu\text{m}/125\ \mu\text{m}$,细芯光纤的芯径为 $5.5\ \mu\text{m}/125\ \mu\text{m}$ 。石墨烯量子点由苏州碳丰石墨烯科技有限公司生产,聚乙烯醇购于国药集团化学试剂有限公司。温湿度传感器的具体制备过程如下:

1) 在 2 cm 长细芯光纤的两端分别熔接两段长度均为 2 mm 的多模光纤,多模光纤的两端再与单模光纤熔接。

2) 将细芯光纤放入特种光纤熔接机中,将熔接机设置为拉锥模式,并将传感器中心部分的细芯光纤放置于熔接机的中心位置;然后选择分步拉锥模式,设置拉锥参数分别为 125、100、70 μm ,放电强度分别为



-20、-50、-70 bits。拉锥部分示意图如图 1(a)所示,整个拉锥部分的长度约为 2 mm,最细部分为 70 μm 。细芯光纤拉锥前后的光谱如图 2 所示。

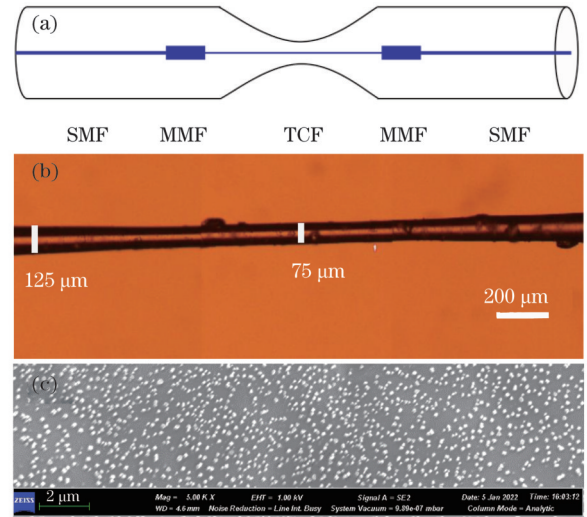


图 1 传感结构。(a)传感器的结构示意图;(b)显微镜下的传感结构;(c)扫描电镜下的石墨烯量子点

Fig. 1 Sensing structure. (a) Structure schematic of sensor; (b) sensing structure under microscope; (c) graphene quantum dots (GQDs) under scanning electron microscope

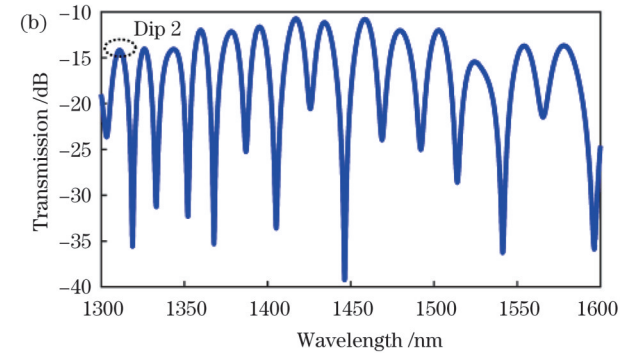


图 2 细芯光纤的初始透射谱。(a)拉锥前;(b)拉锥后

Fig. 2 Initial transmission spectra of thin-core fiber. (a) Before tapering; (b) after tapering

3) 取石墨烯量子点约 5 mg,聚乙烯醇约 100 mg,将二者混合后加入 100 mL 纯净水,然后加热到 95 $^{\circ}\text{C}$ 并保持 1 h,配制成石墨烯量子点-聚乙烯醇溶液;用注射器取 2 mL 溶液,并将其均匀涂覆在细芯光纤锥部,然后将传感器放入真空干燥箱内,设置干燥箱温度为 80 $^{\circ}\text{C}$,在此温度下干燥处理 30 min。在干燥箱的热风作用下,溶液中的溶剂蒸发,最终得到一层附着在传感器锥部的薄膜,其主要成分是聚乙烯醇和石墨烯量子点,如图 1(b)所示,锥部最细部分的直径为 75 μm 。将薄膜放到扫描电子显微镜下进行观察,图 1(c)所示为薄膜中石墨烯量子点的尺寸及分布情况。完全成膜后,再取出结构测试其性能。图 3(a)所示为涂覆石墨烯量子点-聚乙烯醇后传感器的初始透射谱,图 3(b)为涂覆石墨烯量子点-聚乙烯醇后传感器的频谱图。

2.2 传感原理分析

根据光干涉原理,该干涉仪的输出强度 I 可以表示为

$$I = I_{\text{core}} + I_{\text{cladding}} + 2\sqrt{I_{\text{core}}I_{\text{cladding}}}\cos\theta, \quad (1)$$

其中,

$$\theta = \left(\frac{2\pi L\Delta n_{\text{eff}}}{\lambda} \right), \quad (2)$$

式中: I_{core} 和 I_{cladding} 分别表示光纤纤芯模和包层模的光强度; θ 表示芯层和包层的总相位差; L 为细芯光纤拉锥部分的长度; Δn_{eff} 为包层与纤芯的有效折射率差, $\Delta n_{\text{eff}} = n_{\text{eff}}^{\text{cladding}} - n_{\text{eff}}^{\text{core}}$; λ 为入射光波长。

当相位差 $\theta = (2n+1)\pi$ 时,干涉条件成立,由式(2)可得到透射谱谐振峰值波长为

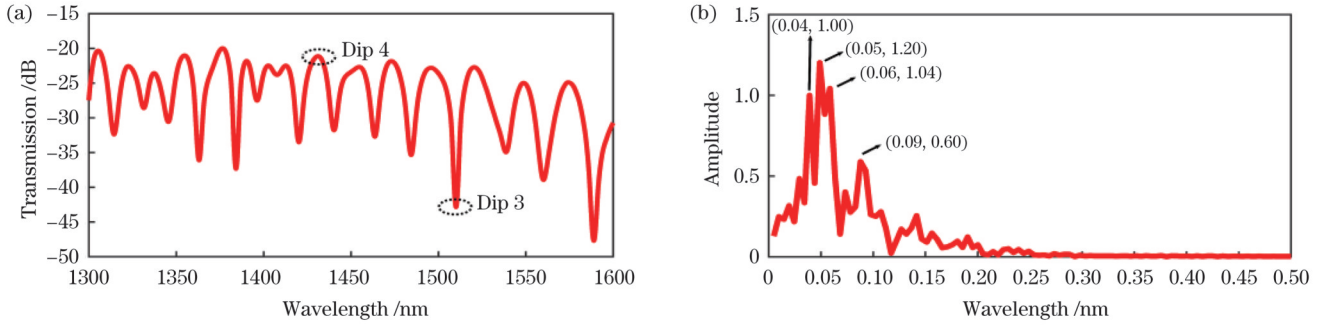


图 3 涂覆石墨烯量子点-聚乙烯醇后传感器的谱线。(a)初始透射谱；(b)频谱分析图

Fig. 3 Spectral lines of sensor after coating with graphene quantum dots-polyvinyl alcohol (GQDs-PVA). (a) Initial transmission spectrum; (b) spectral analysis

$$\lambda_n = \frac{2\Delta n_{eff}L}{2n + 1}, \quad (3)$$

式中： λ_n 表示 n 阶段谐振峰波长。入射光经由单模光纤进入多模光纤后耦合进入细芯光纤，由于中间拉锥部分的光纤直径变细，而且光纤的纤芯与包层厚度都减小，进入的光因纤芯失配而分别在芯层与包层中传输，包层中的光波以倏逝场的形式传输。当光传输到锥形光纤末端时，包层模和纤芯模中的光重新耦合到细芯光纤中输出。由于纤芯和包层的有效折射率不同，锥形光纤中传输的两部分光会形成光程差，构成马赫-曾德尔干涉仪。当拉锥部分被石墨烯量子点-聚乙烯醇涂覆后，由于聚乙烯醇的折射率为 1.52，纯净水的折射率为 1.33，在湿度实验中，随着相对湿度值降低，石墨烯量子点-聚乙烯醇的折射率增加，因此两束干涉光

之间的有效折射率增加，最终导致光谱移动。石墨烯的热效应较强，因此，在温度实验中影响光谱移动的主要因素是石墨烯量子点。通过观察马赫-曾德尔干涉仪在不同温度和相对湿度下的光谱漂移规律，可以测得其相应的温度和相对湿度灵敏度。

3 实验过程与结果分析

3.1 涂覆石墨烯量子点-聚乙烯醇前的温度实验

图 4 所示为温度湿度实验装置示意图。将传感器结构水平拉直并固定在可编程温度湿度试验箱中，将两端的单模光纤分别连接至宽带光源(BBS)与光谱分析仪(OSA)。光谱分析仪型号为 AQ6370D，测量范围为 600~1700 nm，实验温度范围为 30~80 °C。实验时可编程温度湿度试验箱内的相对湿度恒定为 40%。

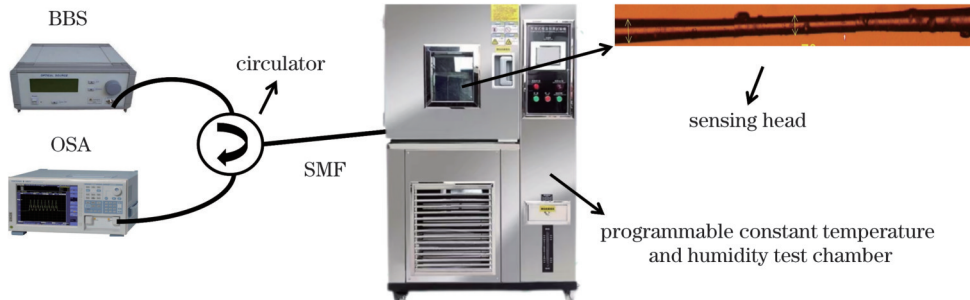


图 4 温度湿度实验装置示意图

Fig. 4 Schematic of temperature and humidity experimental apparatus

拉锥前，随着温度升高(温度变化范围为 30~80 °C)，谐振峰 Dip 1 红移，温度灵敏度为 31 pm/°C，波长与温度的线性拟合度 R^2 为 99.03%，如图 5(a)、(b) 所示。拉锥后，谐振峰 Dip 2 的温度漂移表现如图 5(c) 所示，温度的变化范围仍然保持在 30~80 °C 之间；如图 5(d) 所示，温度灵敏度为 72.7 pm/°C，波长与温度的线性拟合度 R^2 为 98.57%。拉锥前后，线性度均表现良好。

3.2 涂覆石墨烯量子点-聚乙烯醇后的温度实验

将混合好的石墨烯量子点-聚乙烯醇均匀涂覆在传感结构细芯光纤的锥部，涂覆后将该段结构放置在

真空干燥箱中加热至 80 °C，并保持 30 min。当石墨烯量子点-聚乙烯醇呈薄膜状附着在锥部时，将传感器结构水平拉直并固定在可编程温度湿度试验箱中，箱内相对湿度恒定为 40%，传感器两端的单模光纤分别连接至 BBS 和 OSA。在 28~64 °C 的温度范围内，温度每上升 4 °C 记录一次传感器的透射谱，记录的透射谱如图 6 所示。可见，随着温度升高，谐振峰 Dip 3 红移。然后将温度从 64 °C 降低至 28 °C，温度每下降 4 °C 记录一次透射谱。在 48 °C 时，每间隔 10 min 记录一次透射谱，共记录 9 次透射谱，以分析传感器的稳定性。

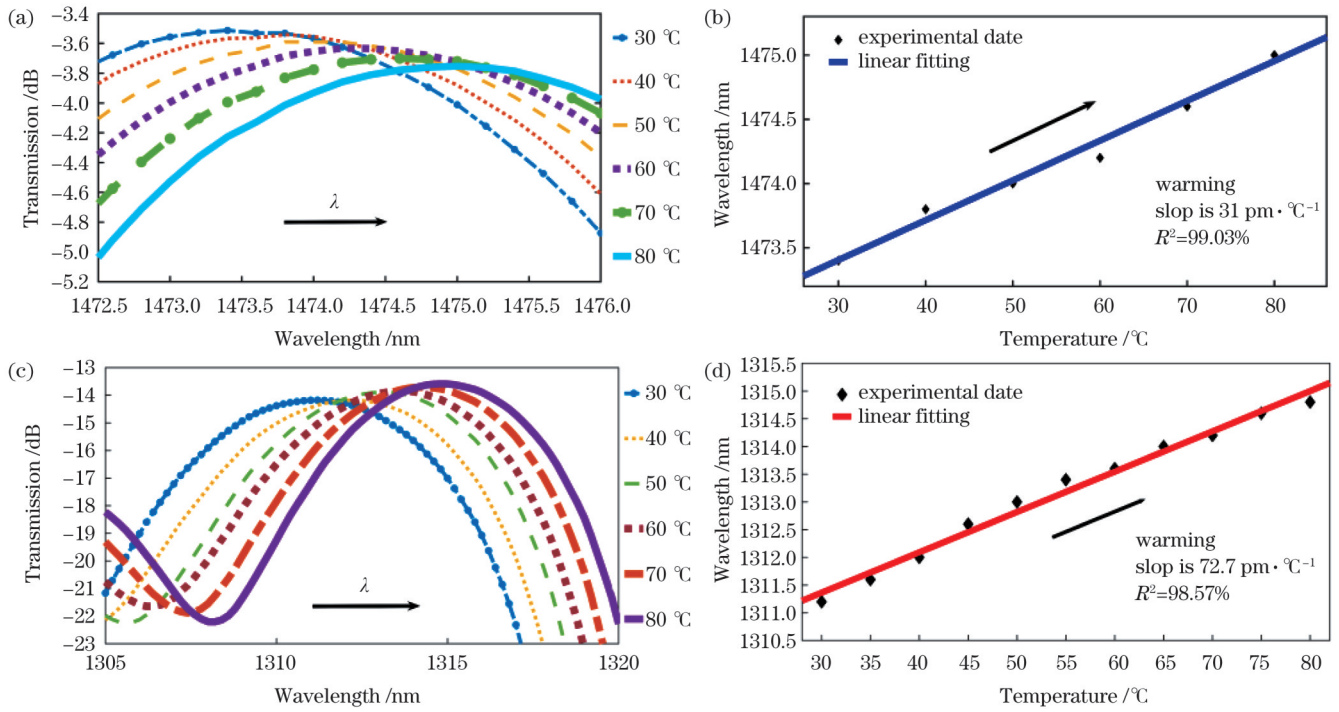


图 5 拉锥前后传感器的温度实验结果。(a)拉锥前的温度漂移;(b)拉锥前的温度拟合;(c)拉锥后的温度漂移;(d)拉锥后的温度拟合
Fig. 5 Temperature experimental results of sensor before and after tapering. (a) Temperature drift before tapering; (b) temperature fitting before tapering; (c) temperature drift after tapering; (d) temperature fitting after tapering

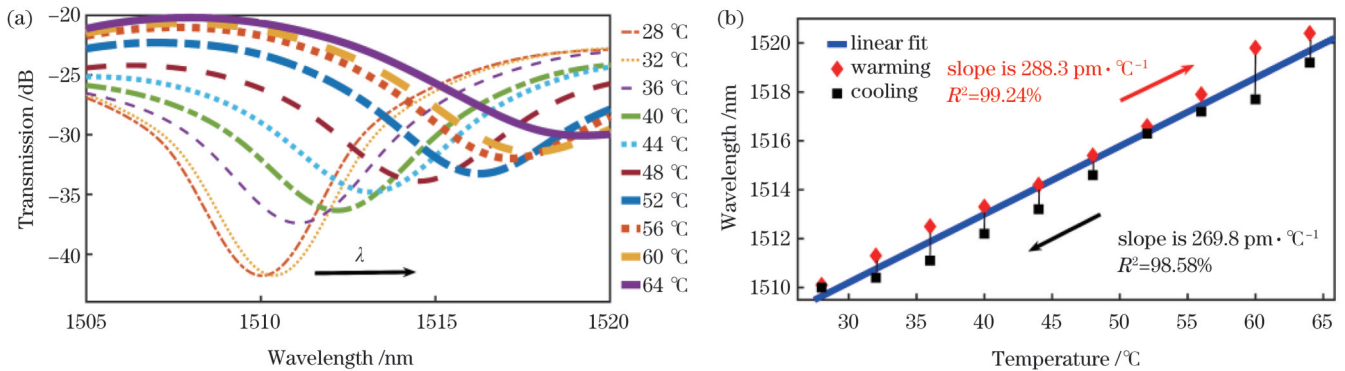


图 6 涂覆石墨烯量子点-聚乙烯醇后传感器的温度实验结果。(a)温度漂移;(b)温度拟合

Fig. 6 Temperature experimental results of sensor after coating GQDs-PVA. (a) Temperature drift; (b) temperature fitting

拉锥后,传感结构的温度灵敏度由拉锥前的 $31 \text{ pm}/^\circ\text{C}$ 提升至 $72.7 \text{ pm}/^\circ\text{C}$;涂覆石墨烯量子点-聚乙烯醇后,温度灵敏度提升至 $288.3 \text{ pm}/^\circ\text{C}$,波长与温度的线性拟合度 R^2 为 99.24% ,如图 6(b)所示。同时,由图 6(b)还可以看出,温度上升和下降过程的重复性较好。当温度为 48°C 时,每间隔 10 min 记录的 9 组数据中,传感器中心波长 1515.5 nm 处的峰值几乎不发生漂移,如图 7 所示。这说明传感器的稳定性较好。

3.3 湿度实验

湿度实验装置与温度实验装置相同,固定温度为 40°C ,以 3% 为步长将相对湿度由 40% 逐步增大到 64% ,每改变一次相对湿度记录一组数据;然后以同样的步长将相对湿度由 64% 降至 40% 。另外,在相对湿度分别为 52% 和 58% 时,每隔 10 min 记录一组数据,

用于测试传感器件的稳定性。

如图 8(a)所示,随着相对湿度增大,谐振峰 Dip 4 红移。由图 8(b)可知:在相对湿度增大(由 40% 增至 64%)实验中,相对湿度灵敏度最高可达到 $131.7 \text{ pm}/\%$,波长与相对湿度的线性拟合度 R^2 为 98.11% ;在相对湿度下降(由 64% 降至 40%)实验中,相对湿度灵敏度为 $125 \text{ pm}/\%$,波长与相对湿度的线性拟合度 R^2 为 98.11% 。这一结果说明在细芯锥部涂覆石墨烯量子点-聚乙烯醇之后,器件对环境相对湿度表现出了线性响应。该传感器镀膜前对湿度并不敏感,镀膜后的相对湿度灵敏度明显提升。如图 9 所示,在环境相对湿度保持为 52% 和 58% 时,传感器中心波长在 1444.2 、 1445.2 nm 处的峰值几乎不发生漂移。这说明该传感器具有优良的稳定性。

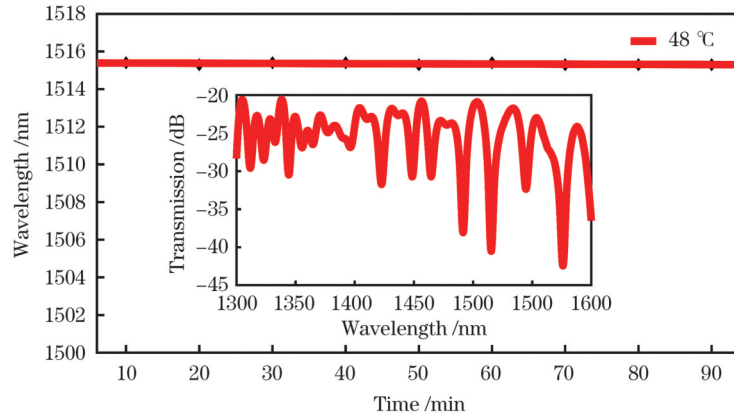


图 7 涂覆石墨烯量子点-聚乙烯醇后传感器的温度稳定性

Fig. 7 Temperature stability of sensor after coating GQDs-PVA

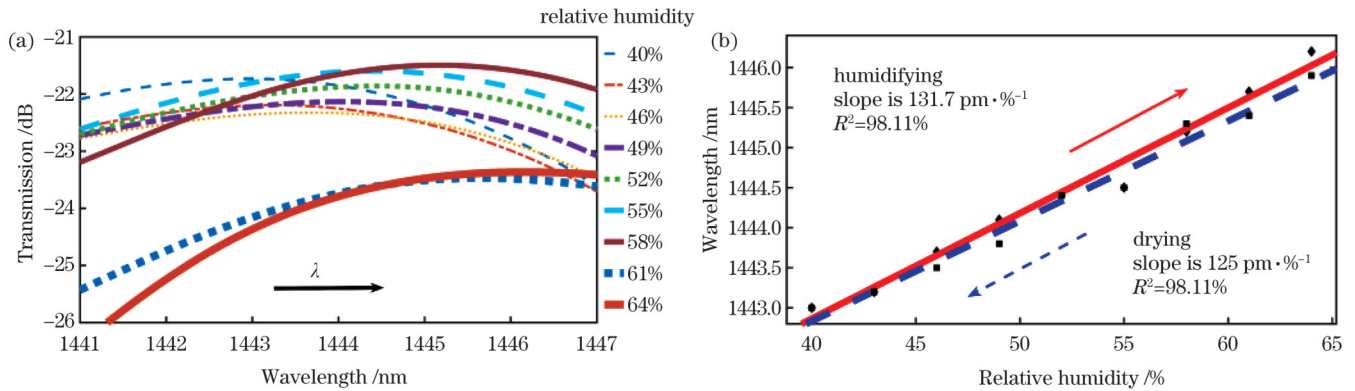


图 8 涂覆石墨烯量子点-聚乙烯醇后传感器的湿度实验结果。(a)相对湿度漂移;(b)相对湿度拟合

Fig. 8 Humidity experimental results of sensor after coating GQDs-PVA. (a) Relative humidity drift; (b) relative humidity fitting

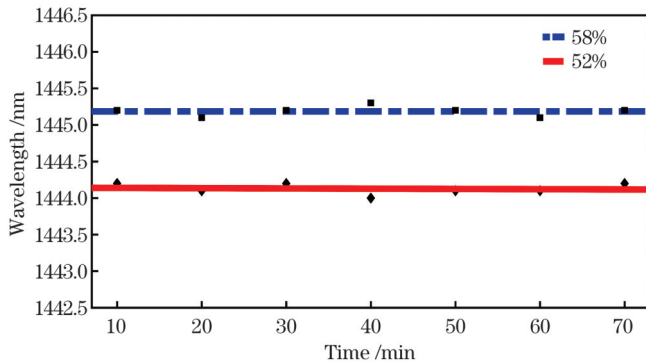


图 9 涂覆石墨烯量子点-聚乙烯醇后传感器的湿度稳定性

Fig. 9 Humidity stability of sensor after coating GQDs-PVA

4 结 论

本团队设计并制备了一款基于表面涂覆石墨烯量子点-聚乙烯醇的锥形细芯光纤的温湿度传感器。实验结果表明:拉锥之前细芯光纤传感器的温度灵敏度为 $31 \text{ pm}/^\circ\text{C}$,拉锥之后的温度灵敏度可达到 $72.7 \text{ pm}/^\circ\text{C}$;将石墨烯量子点-聚乙烯醇涂覆到细芯光纤锥部后,传感器的温度灵敏度可提升到 $288.3 \text{ pm}/^\circ\text{C}$,波长与温度的线性拟合度 R^2 为 99.24% ,相对湿度灵敏度可达到 $137.1 \text{ pm}/\%$,波长与相对湿度的线性拟合度 R^2 为

98.11% 。该传感器具有成本低、灵敏度较高的特点,而且稳定性与重复性均表现良好,在温度与湿度传感领域具有较为广阔的应用前景。

参 考 文 献

- [1] Li C W, Yang S T, Guo Y, et al. Flexible, multi-functional sensor based on all-carbon sensing medium with low coupling for ultrahigh-performance strain, temperature and humidity sensing[J]. Chemical Engineering Journal, 2021, 426: 130364.
- [2] Fu H Y, Zhang S W, Chen H, et al. Graphene enhances the sensitivity of fiber-optic surface plasmon resonance biosensor[J]. IEEE Sensors Journal, 2015, 15(10): 5478-5482.
- [3] Ho M L, Wang J C, Wang T Y, et al. The construction of glucose biosensor based on crystalline iridium(III)-containing coordination polymers with fiber-optic detection[J]. Sensors and Actuators B: Chemical, 2014, 190: 479-485.
- [4] Zhang L Y, Zhang W G, Chen L, et al. A fiber bending vector sensor based on M-Z interferometer exploiting two hump-shaped tapers[J]. IEEE Photonics Technology Letters, 2015, 27(11): 1240-1243.
- [5] Mobini E, Mafi A. Design of a wavelength-tunable optical tweezer using a graded-index multimode optical fiber[J]. Journal of Lightwave Technology, 2017, 35(18): 3854-3861.
- [6] Wo J H, Sun Q Z, Liu H, et al. Sensitivity-enhanced fiber optic temperature sensor with strain response suppression[J]. Optical Fiber Technology, 2013, 19(4): 289-292.
- [7] Hu H F, Sun S J, Lü R Q, et al. Design and experiment of an optical fiber micro bend sensor for respiration monitoring[J]. Sensors and Actuators A: Physical, 2016, 251: 126-133.

- [8] Xiao H L, Cui X L, Lei W K. A bored pile deficiency detection method based on optical fiber temperature measurement[J]. *Optical Fiber Technology*, 2015, 21: 1-6.
- [9] Fu D Y, Liu X J, Shang J Y, et al. A simple, highly sensitive fiber sensor for simultaneous measurement of pressure and temperature[J]. *IEEE Photonics Technology Letters*, 2020, 32(13): 747-750.
- [10] Kuang G F, Kuang C L. Construction of intelligent lighting system of vehicle based on optical fiber sensors technology[C] // *Proceedings of the 2016 International Conference on Education, Management and Computer Science, Advances in Intelligent Systems Research*, May 27-29, 2016, Shenyang, China. Paris: Atlantis Press, 2016: 482-486.
- [11] Chen Q Y, Chen Q Y, et al. Fiber Bragg gratings and their applications as temperature and humidity sensors[J]. *Atomic, Molecular and Optical Physics*, 2008, 6: 235.
- [12] Zhang J X, Shen X Y, Qian M, et al. An optical fiber sensor based on polyimide coated fiber Bragg grating for measurement of relative humidity[J]. *Optical Fiber Technology*, 2021, 61: 102406.
- [13] Zhang C, Zhang W, Webb D J, et al. Optical fibre temperature and humidity sensor[J]. *Electronics Letters*, 2010, 46(9): 643-644.
- [14] 石胜辉, 吴德操, 王鑫, 等. 氧化石墨烯包覆金纳米壳修饰长周期光栅的免疫传感器[J]. *光学学报*, 2020, 40(18): 1806001.
- [15] Shi S H, Wu D C, Wang X, et al. An immunosensor based on the graphene-oxide-encapsulated Au-nanoshell-coated long-period fiber grating[J]. *Acta Optica Sinica*, 2020, 40(18): 1806001.
- [16] Zhang S Q, Dong X Y, Li T, et al. Simultaneous measurement of relative humidity and temperature with PCF-MZI cascaded by fiber Bragg grating[J]. *Optics Communications*, 2013, 303: 42-45.
- [17] Soltanian M R K, Sharbirin A S, Ariannejad M M, et al. Variable waist-diameter Mach - Zehnder tapered-fiber interferometer as humidity and temperature sensor[J]. *IEEE Sensors Journal*, 2016, 16(15): 5987-5992.
- [18] Li J X, Tong Z R, Jing L, et al. Fiber temperature and humidity sensor based on photonic crystal fiber coated with graphene oxide [J]. *Optics Communications*, 2020, 467: 125707.
- [19] Chen N, Liu C N, Lu Z Q, et al. Femtosecond laser processing for a high sensitivity fiber MZI microcavity[J]. *Optics Express*, 2022, 30(8): 12397-12408.
- [20] Ohodnicki P R, Jr, Brown T D, Holcomb G R, et al. High temperature optical sensing of gas and temperature using Au-nanoparticle incorporated oxides[J]. *Sensors and Actuators B: Chemical*, 2014, 202: 489-499.
- [21] Bai Y, Yan F P, Feng T, et al. Temperature fiber sensor based on single longitudinal mode fiber laser in 2 μm band with Sagnac interferometer[J]. *Optical Fiber Technology*, 2019, 51: 71-76.
- [22] Lei X Q, Dong X P. High-sensitivity Fabry - Perot interferometer high-temperature fiber sensor based on vernier effect[J]. *IEEE Sensors Journal*, 2020, 20(10): 5292-5297.
- [23] Shin J C, Yoon M S, Han Y G. Relative humidity sensor based on an optical microfiber knot resonator with a polyvinyl alcohol overlay [J]. *Journal of Lightwave Technology*, 2016, 34(19): 4511-4515.
- [24] Ma Q F, Tou Z Q, Ni K, et al. Carbon-nanotube/polyvinyl alcohol coated thin-core fiber sensor for humidity measurement[J]. *Sensors and Actuators B: Chemical*, 2018, 257: 800-806.
- [25] 邓理, 张建奇, 孙浩, 等. 基于静电纺丝纳米纤维膜的光纤湿度传感器[J]. *激光与光电子学进展*, 2021, 58(9): 0906006.
- [26] Deng L, Zhang J Q, Sun H, et al. Optical fiber temperature and humidity sensor based on film prepared by electrospinning nanofibers[J]. *Laser & Optoelectronics Progress*, 2021, 58(9): 0906006.
- [27] Novais S, Ferreira M S, Pinto J L. Relative humidity fiber sensor based on multimode interferometer coated with agarose-gel[J]. *Coatings*, 2018, 8(12): 453.
- [28] Zeng H Y, Shen C Y, Lu Y F, et al. Refractive index sensor based on polarization-maintaining fiber M-Z interferometer with an FBG[J]. *Chinese Journal of Sensors and Actuators*, 2015, 28(11): 1727-1731.
- [29] 黄如霞, 王越, 周文超, 等. 非绝热结构模式干涉高灵敏度光纤传感器[J]. *光学学报*, 2021, 41(23): 2306001.
- [30] Huang R X, Wang Y, Zhou W C, et al. High-sensitivity interferometric fiber sensor with non-adiabatic structure mode[J]. *Acta Optica Sinica*, 2021, 41(23): 2306001.
- [31] Liu Y G, Liu X, Zhang T, et al. Integrated FPI-FBG composite all-fiber sensor for simultaneous measurement of liquid refractive index and temperature[J]. *Optics and Lasers in Engineering*, 2018, 111: 167-171.
- [32] 徐施施, 冯文林. 基于薄芯-三芯细锥-薄芯光纤结构的应变传感器[J]. *光学学报*, 2020, 40(18): 1806002.
- [33] Xu S S, Feng W L. Strain sensor based on thin-core-tapered three cores-thin-core fiber structure[J]. *Acta Optica Sinica*, 2020, 40(18): 1806002.
- [34] 刘靖阳, 王涛, 张倩, 等. BOTDA 系统温度应变双参量传感技术研究进展[J]. *激光与光电子学进展*, 2021, 58(13): 1306021.
- [35] Liu J Y, Wang T, Zhang Q, et al. Research progress on temperature-strain dual-parameter sensing in BOTDA system[J]. *Laser & Optoelectronics Progress*, 2021, 58(13): 1306021.
- [36] Lu P, Men L Q, Sooley K, et al. Tapered fiber Mach-Zehnder interferometer for simultaneous measurement of refractive index and temperature[J]. *Applied Physics Letters*, 2009, 94(13): 131110.
- [37] Gong J Q, Shen C Y, Xiao Y K, et al. High sensitivity fiber temperature sensor based PDMS film on Mach-Zehnder interferometer[J]. *Optical Fiber Technology*, 2019, 53: 102029.
- [38] Vaz A, Barroca N, Ribeiro M, et al. Optical fiber humidity sensor based on polyvinylidene fluoride Fabry - Perot[J]. *IEEE Photonics Technology Letters*, 2019, 31(7): 549-552.
- [39] 徐妍妍, 李俊, 李浩, 等. 基于拉锥七芯光纤的湿度传感器研究[J]. *中国激光*, 2021, 48(23): 2306002.
- [40] Xu Y Y, Li J, Li H, et al. Research on humidity sensor based on tapered seven core fiber[J]. *Chinese Journal of Lasers*, 2021, 48(23): 2306002.
- [41] Lu H, Li W, Dong H, et al. Graphene quantum dots for optical bioimaging[J]. *Small*, 2019, 15(36): 1902136.
- [42] Sahub C, Tuntulani T, Nhujak T, et al. Effective biosensor based on graphene quantum dots via enzymatic reaction for directly photoluminescence detection of organophosphate pesticide[J]. *Sensors and Actuators B: Chemical*, 2018, 258: 88-97.
- [43] Aslam M, Kalyar M A, Raza Z A. Polyvinyl alcohol: a review of research status and use of polyvinyl alcohol based nanocomposites [J]. *Polymer Engineering & Science*, 2018, 58(12): 2119-2132.
- [44] Wong W C, Chan C C, Chen L H, et al. Polyvinyl alcohol coated photonic crystal optical fiber sensor for humidity measurement[J]. *Sensors and Actuators B: Chemical*, 2012, 174: 563-569.

Temperature and Humidity Sensor Based on Tapered Thin-Core Fiber Coated with Graphene Quantum Dots-Polyvinyl Alcohol

Lu Zhiqi, Dong Ruimin, Liu Changning*

College of Physics and Electronic Science, Hubei Normal University, Huangshi 435002, Hubei, China

Abstract

Objective Temperature and relative humidity sensors play an important role in various processes. Compared with traditional sensors, optical fiber sensors have the advantages of simple structure, strong corrosion resistance, and strong anti-electromagnetic interference capability. Functional sensors reduce manufacturing difficulty and cost compared to non-functional sensors because they do not require other sensitive components. Among them, interferometric sensors have become a topic of interest in recent years because of their simple manufacturing process and low cost. In particular, the Mach-Zehnder interferometer (MZI) plays an indispensable role in the measurement of basic physical quantities, such as temperature, relative humidity, refractive index, and stress. However, indicators such as the sensitivity and stability of MZI sensors need to be improved. To further improve the sensitivity and stability of such sensors, we propose and demonstrate a temperature and relative humidity sensor based on a tapered thin-core fiber coated with a graphene quantum dots-polyvinyl alcohol (GQDs-PVA) solution. The sensor consists of a 2 cm segment of tapered thin-core fiber and two 2 mm multi-mode fibers. The two multimode fibers are located between two single-mode fibers, in which the thin-core fiber constitutes the sensor cone after distributed taper processing. When the external temperature, relative humidity, and other physical quantities vary, the effective refractive index difference between the cladding and core layers changes, resulting in the movement of the central wavelength of the spectral line, which can be monitored in real time on the spectrometer. Therefore, this optical fiber sensor can monitor changes in these external physical quantities. The proposed sensor exhibits higher temperature sensitivity after coating with the GQDs-PVA solution than traditional sensors. In addition, owing to the unique properties of PVA, the sensor exhibits high sensitivity to relative humidity. Compared to other sensors intended to measure these quantities, this sensor is more effective and less expensive. The sensor is characterized by high sensitivity and stability, and thus, it is a suitable candidate for research and practical applications.

Methods First, two segments of multi-mode fiber (MMF) with a length of 2 mm were spliced onto both sides of a 2 cm segment of thin-core fiber (TCF) using a fiber fusion machine. Single-mode fibers (SMFs) were then fused to both sides of the TCF. The thin-core fiber was then placed in the special optical fiber fusion machine (FSM-100P +), the taper mode was selected to provide a distributed taper, the center position of the thin-core fiber was aligned with the center of the special optical fiber fusion machine, and the diameter of the thin-core fiber was initially tapered from 125 μm to 100 μm and finally to 70 μm ; discharge amounts were -20 , -50 , and -70 bits. Finally, graphene quantum dots (GQDs) and polyvinyl alcohol (PVA) were thoroughly mixed and the GQDs-PVA solution was evenly applied to the sensor cone. The sensor was placed horizontally in a vacuum oven and heated at 80 $^{\circ}\text{C}$ for 30 min. After the heating process, the GQDs-PVA mixed solution adhered to the sensor surface in the form of a film. The particle size and distribution of the GQDs were examined using scanning electron microscopy (SEM). The structure was placed in a programmable constant temperature and relative humidity experimental chamber before and after taper pulling to test the effect of temperature and relative humidity on the sensor spectra. The stability and repeatability of the structure were also tested, and its sensitivity and linearity, based on several experiments, were evaluated.

Results and Discussions First, we performed temperature experiments on the experimental samples before and after tapering the thin-core fiber, and the temperature sensitivity of the sensor was measured to be 31 $\text{pm}/^{\circ}\text{C}$ and 72.7 $\text{pm}/^{\circ}\text{C}$, respectively (Fig. 5). The GQDs-PVA mixture solution was then evenly applied to the sensor cone, and the temperature sensitivity increased to 288.3 $\text{pm}/^{\circ}\text{C}$ after application of the solution (Fig. 6). In addition, the refractive index of the PVA solution changed according to the ambient relative humidity, and the sensitivity of the sensor to ambient relative humidity was 131.7 $\text{pm}/\%$ after coating with the GQDs-PVA solution (Fig. 8). We also tested the repeatability and stability of the sensor after coating. As the temperature (Fig. 6) and relative humidity (Fig. 8) varied, the sensitivity showed little deviation and the sensor exhibits good repeatability. When the temperature was 48 $^{\circ}\text{C}$, the peak at 1515.5 nm of the central wavelength of the sensor exhibited minimal shift (Fig. 7). When the relative humidity was 52% and 58%, the center wavelength of the sensor drifted (1442.2 nm and 1445.2 nm, respectively), indicating that the sensor was sensitive and exhibited good stability and repeatability with respect to both temperature and relative humidity.

Conclusions In summary, we propose and demonstrate a temperature and relative humidity sensor based on tapered thin-core fibers coated with GQDs-PVA. The experimental results indicate that the temperature sensitivity of tapered thin-core fibers can be increased to $72.7 \text{ pm}/^{\circ}\text{C}$, and it can be further increased to $288.3 \text{ pm}/^{\circ}\text{C}$ after surface application of the GQDs-PVA mixed solution, which makes the sensor 9.3 times more sensitive than the uncoated device. The relative humidity sensitivity of the proposed sensor is also higher than that of other types of Mach-Zehnder interferometer (MZI) sensors. Because PVA absorbs water and changes its refractive index when the ambient relative humidity changes, it changes the effective refractive index difference between the cladding and the core, which in turn causes a beneficial spectrum drift. Therefore, the coated sensor exhibits an ambient relative humidity sensitivity of $131.7 \text{ pm}/\%$ instead of the complete insensitivity at the beginning. The GQDs-PVA sensor has a simple structure, good stability, high sensitivity, and is a good candidate in the field of temperature and relative humidity sensing.

Key words sensors; thin-core fibers; graphene quantum dots (GQDs); polyvinyl alcohol (PVA); temperature; relative humidity